Optically detected magnetic resonance study of an oxygen-vacancy complex in BaFBr

1995 J. Phys.: Condens. Matter 7 6925

(http://iopscience.iop.org/0953-8984/7/34/015)

J. Phys.: Condens. Matter 7 (1995) 6925–6937. Printed in the UK

Optically detected magnetic resonance study of an oxygen–vacancy complex in BaFBr

F K Koschnick†, Th Hangleiter†, K S Song† and J-M Spaeth‡
† Fachbereich Physik, University of Paderborn, 33095 Paderborn, Germany
‡ Department of Physics, University of Ottawa, Ottawa, Ontario K1N 6N5, Canada

Received 20 May 1995

Abstract. BaFBr is usually contaminated with oxygen which influences the performance of this well known x-ray storage phosphor material. Oxygen is incorporated as a diamagnetic O^{2-} ion on F^- sites with a nearby charge-compensating vacancy in the Br^- sublattice, as is known from the paramagnetic O_F^- and $F(Br^-)$ centres created by room-temperature x-irradiation and studied in detail with electron paramagnetic resonance (EPR) techniques. It is shown that BaFBr:O_F^{2-} has a luminescence band excited at 4.95 eV, peaking at 2.43 eV with two radiative lifetimes of 0.2 ms and 1 ms, respectively. With luminescence-detected EPR (i.e. optically detected magnetic resonance (ODMR)), it is shown that the luminescence is due to an excited triplet state of an O_F^{2-}–Br^- vacancy pair. Time-resolved ODMR measurements reveal the same radiative lifetimes as seen in luminescence. No singlet emission was observed. The zero-field splitting can be explained assuming a $F(Br^-)$–O_F^- pair defect as the excited triplet state.

1. Introduction

Barium fluorobromide crystallizes in the PbFCl structure, as shown in figure 1 (Liebig and Nicollin 1977, Beck 1979). Doping of europium as an activator ion makes this material one of the best x-ray storage phosphors. Eachus *et al* (1991a,b) showed that a nominally undoped BaFBr crystal is heavily contaminated with oxygen. It is very difficult to avoid this contamination. Oxygen is incorporated as O^{2-} with a charge-compensating vacancy in the halide sublattice. O^{2-} acts as a hole trap. When creating V_K centres (Br_2^-) by x-irradiation at low temperatures and warming above 120 K, where the B_2^-–V_K centres become mobile, O^{2-} catches a hole and becomes the paramagnetic O^- ion. By electron paramagnetic resonance (EPR) and electron nuclear double resonance (ENDOR) it was shown that O^- resides on a substitutional F^- site (Eachus *et al* 1991a,b). After the production of O_F^- defects by x-irradiation at room temperature, no indication was found that the O_F^- defect might be perturbed by a charge-compensating vacancy. Within experimental error of the ENDOR measurements, the symmetry of the O_F^- defects is D_{2d} (Eachus *et al* 1991b). X-irradiation at room temperature also generates unperturbed $F(Br^-)$ centres (i.e. electron trap centres at Br^- sites). However, x-irradiation at 4.2 K produced perturbed $F(Br^-)$ but no O_F^- defects. Annealing to 120 K produced perturbed O_F^- centres and $F(Br^-)$ centres. The perturbance is seen from a slight energy shift of the optical absorption bands. Both defects convert simultaneously to unperturbed states by further annealing to a temperature above 200 K where the $F(Br^-)$ centres and Br^- vacancies can diffuse away from the oxygen (Koschnick 1991).

These experiments were interpreted by assuming that O_F^{2-} is incorporated with a spatially correlated Br^- vacancy at the nearest or second-nearest Br^- site, the correlation being

0953-8984/95/346925+13$19.50

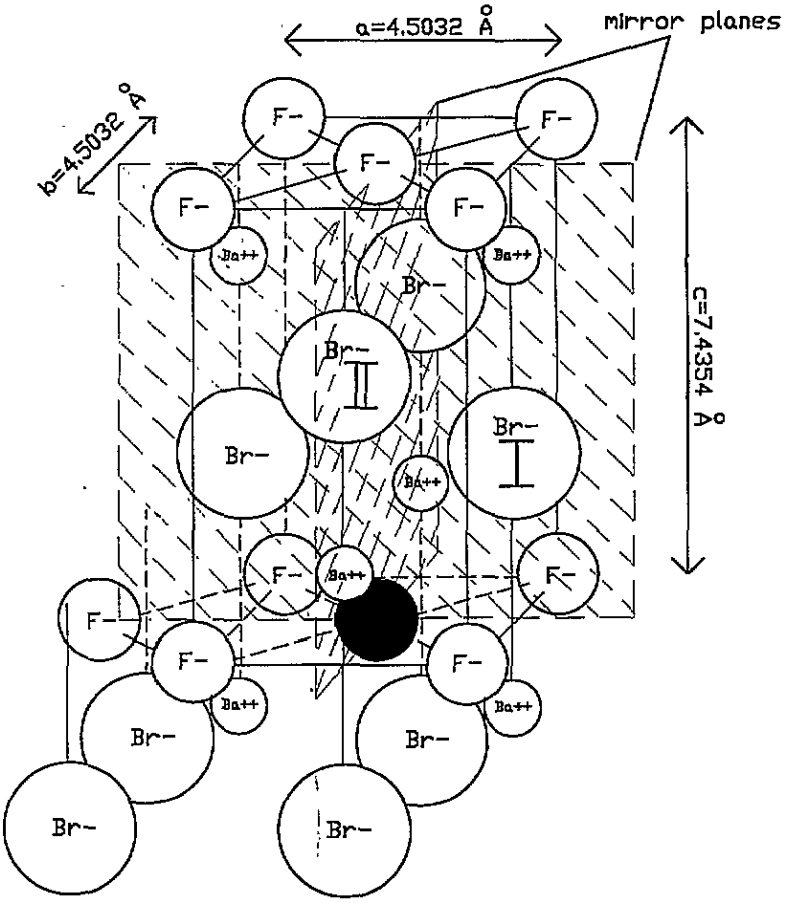

Figure 1. Crystal structure of BaFBr with the oxygen atom on an F^- site (full circle). The positions of the nearest (Br_I) and the second-nearest (Br_{II}) neighbours are indicated as well as the two mirror planes $c-a$ and $c-b$.

stabilized by Coulomb forces between O^{2-} and the positive Br^- vacancy. After trapping an electron in the Br^- vacancy, i.e. forming an $F(Br^-)$ centre, the vacancy becomes neutral and can diffuse away above 200 K. Also, the Br^- vacancy can diffuse away after O_F^{2-} has caught a hole. Therefore, unperturbed $F(Br^-)$ and O_F^- centres are observed.

It was the purpose of this paper to study the O^{2-} defect in more detail. Since the oxygen contamination, even at very low concentrations, greatly influences the performance of the x-ray storage phosphor $BaFBr:Eu^{2+}$ (Spaeth *et al* 1995), a sensitive method to detect the oxygen contamination is very important. In oxygen containing BaFBr a luminescence band peaking at about 500 nm was discovered, which was tentatively assigned to O_F^{2-} (Koschnick 1991). This band was previously observed by Crawford and Brixner (1989) who speculated that this luminescence was due to a self-trapped exciton (STE) in the bromide sublattice. We shall show that this luminescence comes indeed from an excited triplet state of substitutional O^{2-} perturbed by a nearby Br^- vacancy.

2. Experimental procedures

Single crystals of BaFBr were grown by the Bridgman method in graphite crucibles. Mixtures of optical-grade zone-refined BaF_2 and $BaBr_2$ treated with $SiBr_4$ to remove oxygen were grown under argon gas at 200 mbar.

It turned out that the $SiBr_4$ treatment did not suffice to remove all oxygen from BaFBr. Those crystals are called 'normally grown' crystals. One crystal was treated at 800 °C in a vitreous carbon boat with HF–Ar gas flow for 3 h. The vitreous carbon boat was in a sealed vitreous carbon tube. After this treatment, the material was cooled to room temperature in a dry Ar gas flow. Then, the material was filled into the growth crucible under dry Ar conditions in a glove-box. Before single-crystal growth, the crucible was sealed. The resulting crystals contained very little oxygen (see section 3). Some crystals were doped deliberately with dried unhydrogenous BaO for oxygen doping.

The optical measurements including luminescence-detected EPR (optically detected magnetic resonance (ODMR)) were performed with a custom-built computer-controlled ODMR spectrometer operating at 24 GHz described previously (Ahlers *et al* 1983). The excitation measurements of the luminescence were performed with a deuterium lamp and a 0.25 m double monochromator. A photomultiplier and a lock-in amplifier were used as detectors. The excitation and luminescence spectra were corrected for the spectral response of the monochromator, for the lamp intensity, and for the detector sensitivity. The excitation for the ODMR measurements was done with the deuterium lamp in connection with an interference filter with 25% transmission at 251 nm and a half-width of about 21 nm. The luminescence lifetime measurement for lifetime measurement longer than 30 μs was performed with a PC-controlled transient recording board triggered by the chopper for the excitation light. The decay time of the mechanical chopper in connection with a pinhole was about 30 ns. The measured lifetimes were long enough to neglect the decay time of the chopper. 2000 scans were performed and integrated simultaneously with the PC. Lifetime measurements for times between 10 ns and 300 μs were done with a photon-counting set-up using a fast photomultiplier as detector.

The ODMR signal was detected as microwave-induced change in the luminescence intensity integrally measured with a band edge filter of about 418 nm. The time-resolved ODMR measurements were performed with the same transient recording board used for the lifetime measurements above 30 μs. The microwave switch controller was used as the trigger. As a microwave switch a p–i–n diode was used. The ODMR effect was monitored with time resolution by switching the microwave power on and off. 10 000 scans for each cycle (switching on and off the microwave power) were measured.

3. Experimental results

3.1. Luminescence measurements

The luminescence spectrum excited in the UV of a 'normally grown' crystal is shown in figure 2(a). It peaks at 2.43 ± 0.01 eV and has a half-width of 0.38 ± 0.01 eV. Figure 2(b) presents the corresponding excitation spectrum which is identical with the absorption spectrum having a peak at 4.96 eV (250 nm) within experimental error. The absorption and the luminescence can only be observed in BaFBr crystals which contain oxygen. In table 1 the relative luminescence intensities at 2.43 eV are listed for a crystal nominally doped with 200 ppm BaO, one which was 'normally grown' and one which had the HF purification treatment (see section 2). The luminescence almost disappears in the

purified crystal and is quite strong in the crystal doped with oxygen. Thus, the luminescence cannot be the intrinsic luminescence of a STE as speculated by Crawford and Brixner (1989) but is due to the oxygen impurity. The decay of the luminescence measured at 2.43 eV and 2.0 K reveals two decay times: a short decay time with $\tau_1 = 0.2$ ms and a long decay time with $\tau_2 = 1$ ms (figure 3).

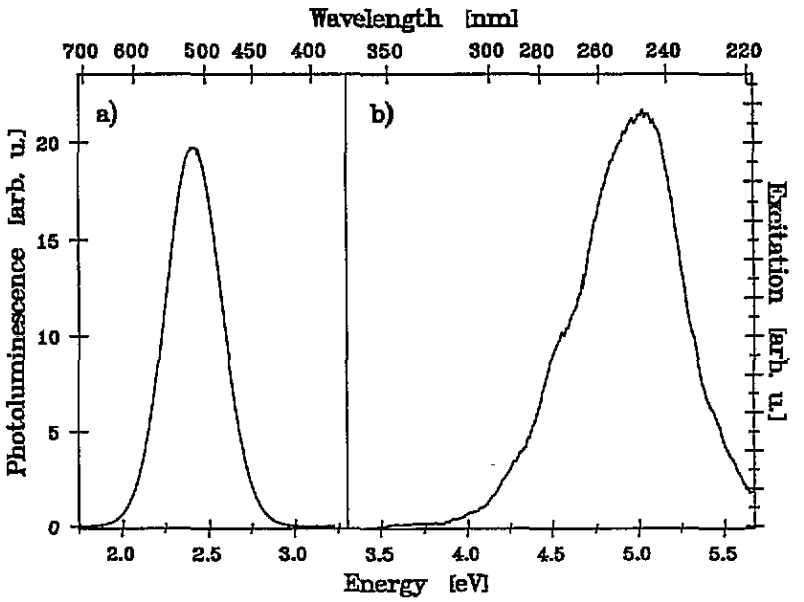

Figure 2. (a) Luminescence spectrum of oxygen-contaminated BaFBr excited at 5 eV and measured at 1.5 K. (b) Excitation spectrum of the luminescence peaking at 2.43 V measured at 1.5 K.

Table 1. Relative luminescence intensities at 2.43 eV for various BaFBr crystals.

Crystal	Luminescence intensity (au)
BaFBr 'oxygen free' purified with HF	17
BaFBr 'normally grown'	320
BaFBr doped with 200 ppm BaO	1650

Precision: approximately ±20%.

The ratio of the intensities of the two lifetime components was estimated to be $A_2(\tau_2 = 1 \text{ ms})/A_1(\tau_1 = 0.2 \text{ ms}) = 1.7$. It will be shown below with the help of time-resolved ODMR measurements that the two different lifetimes result from the different sublevels of the spin triplet of the excited state of the oxygen defect and that we did not measure two different contributions to the luminescence from different defects.

No lifetime component shorter than 0.2 ns was detected. Thus, no singlet luminescence from the excited oxygen was observed.

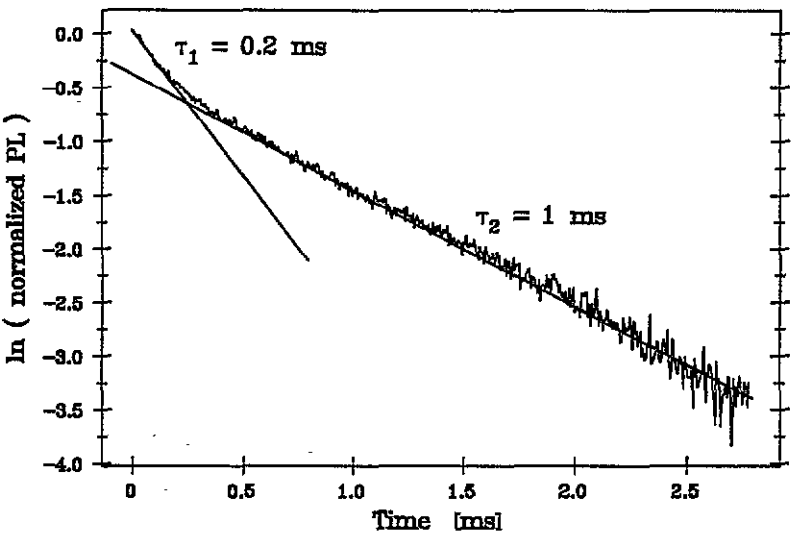

Figure 3. Lifetime measurements of the integral luminescence band peaking at 2.43 eV. The excitation was done with a deuterium lamp and an interference filter (251 nm; bandwidth 21 nm, 25% transmission). The lifetimes are $\tau_1 = 0.2$ ms and $\tau_2 = 1.0$ ms at 2 K. The ratio of the amplitude of the long exponential to that of the short exponential is 1.7.

3.2. Stationary optically detected magnetic resonance measurements

The ground state of O^{2-} is diamagnetic. The oxygen-doped BaFBr crystals therefore showed no EPR spectrum. Figure 4 shows a luminescence-detected ODMR spectrum for the magnetic field B parallel to the c axis. The excited state can become paramagnetic if the excited electron and the remaining unpaired electron have parallel spins, i.e. if the excited O^{2-*} is in a spin triplet state. The spectrum of figure 4 is characteristic for a triplet EPR spectrum with two lines symmetrical about $g \approx 2$ split by the fine-structure interaction. The angular dependence where the magnetic field direction is changed from $B \parallel c \rightarrow B \parallel b$ is shown in figure 5. The crystal axes c, a and b are shown in figure 1. a and b are equivalent crystal axes. The crystal structure of BaFBr is tetragonal with the symmetry group 4p/nmm. The orientation of the crystal was determined by conventional ENDOR measurements of $F(Br^-)$ centres after additive colouration of parts of the same crystal used for the ODMR experiments. The ENDOR signals of these defects are known (Koschnick *et al* 1992). Using the known hyperfine tensors of $F(Br^-)$ centres, the orientation of the BaFBr crystal could be determined very precisely from the measured $F(Br^-)$ ENDOR lines. From x-ray diffraction with the Laue method, the a axis could not be determined unambiguously.

The analysis of the ODMR angular dependence was performed with the following spin Hamiltonian and with the assumption of an $S = 1$ system:

$$H = \mu_B B \cdot \mathbf{g} \cdot S + S \cdot \mathbf{D} \cdot S \tag{1}$$

where $\mathbf{g}$ and $\mathbf{D}$ are the g and D tensor, respectively. μ_B is the Bohr magneton and S is the electron spin operator. The orientations of the g and D tensors were described with a set of Euler angles. In the principal axis system the g tensor can be characterized by its three principal values g_{xx}, g_{yy} and g_{zz}. The D tensor can be expressed with the two values D and E in the principal axis system which have the usual meaning as the axial and non-axial parts, respectively (Abragam and Bleaney 1986).

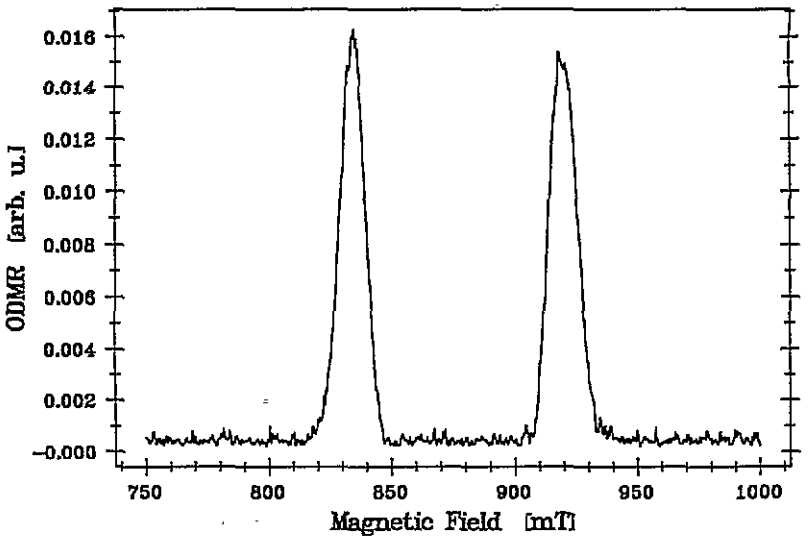

Figure 4. ODMR spectrum measured as a microwave-induced increase in the integral luminescence intensity of figure 2(a) for $B_0 \parallel c$ axis. The luminescence was measured with a band edge filter of 418 nm (2.97 eV). $\nu = 23.9$ GHz, $T = 1.5$ K and luminescence excitation at 251 nm.

The theoretical angular dependences of figure 5 (solid lines) were calculated using equation (1) with the parameters listed in table 2. It turned out that two of the principal axes of the fine-structure tensor are in a mirror plane as indicated in figure 1. Thus, the tensor orientation with respect to the crystal axis is described by one free angle only (see table 2).

Table 2. Parameters of the spin Hamiltonian (equation (1)) of the oxygen–Br^- vacancy pairs in BaFBr obtained from ODMR. D and E are the usual parameters of the fine-structure tensor describing the axial part (D) and the deviation from axial symmetry (E). β_g and β_d describe the angles between the z axes of the g and D tensors, respectively, and the c axis of the crystal. The other two principal axes are determined by the mirror symmetries. The precision of the experimental results is as follows: g factors to ± 0.005; D- and E-values to ± 0.3 mT; β_g and β_d to $\pm 1°$.

g_{zz}	g_{vv}	g_{zz}	β_g (deg)	D (mT)	E (mT)	β_d (deg)
1.98	1.99	1.95	131	77.5	20.7	116

The analysis of the angular dependence of figure 5 yielded that there are four centre orientations. For two orientations, two principal axes are in the mirror plane containing the c and a axes; for the other two orientations they are in the mirror plane containing the c and b axes. When rotating the magnetic field, for example, from the c axis to the a axis in the c–a plane (figure 5, lower half), the two centre orientations in the c–b plane remain equivalent having only one fine-structure split doublet.

Attempts to determine the sign of the zero-field splitting parameter D by measuring the magnetic circular polarization of the emission (MCPE) failed. For $B \parallel c$ the magnetic field is not parallel to a principal axis of the D tensor and therefore the selection rules

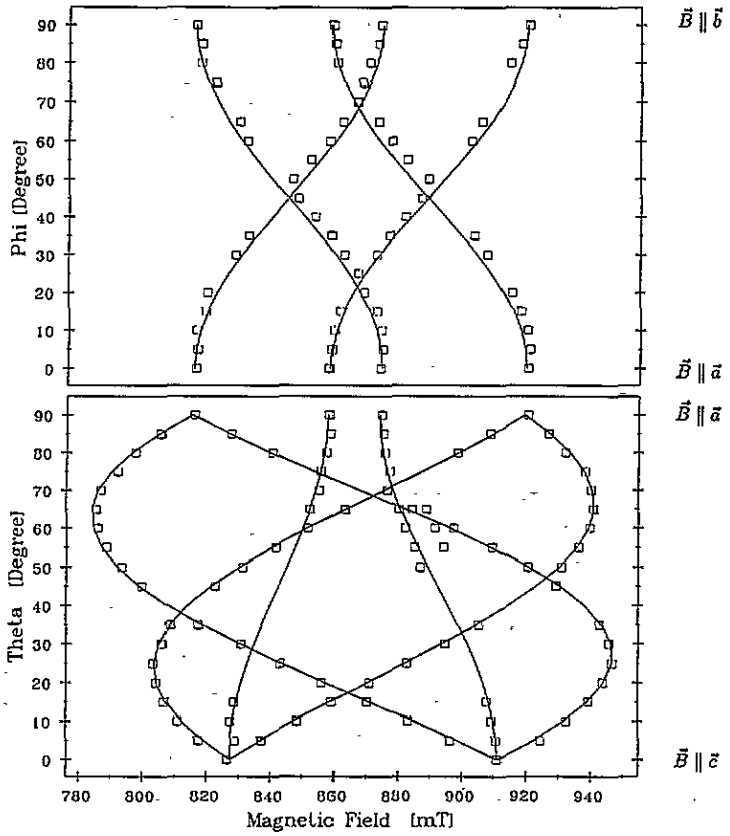

Figure 5. Angular dependence of the ODMR lines of figure 4 measured from $B \parallel c \rightarrow B \parallel a$ (angle θ) and from $B \parallel a \rightarrow B \parallel b$ (angle ϕ). The open squares represent the peak positions of the ODMR lines and the solid lines are the calculated angular dependences using the spin Hamiltonian (equation (1)) and the parameters of table 2.

usually causing the right and left circularly polarized emission from the $|m_s\rangle = \pm 1$ states are not strictly obeyed (there are no pure $|m_s\rangle = \pm 1$ states in this orientation). For other orientations of B, the birefringence of the BaFBr crystal hampered the observation of left or right circularly polarized emissions.

We tried to measure an excitation spectrum of the ODMR lines through the luminescence band ('tagged luminescence') using a monochromator. Unfortunately, the ODMR signal was too weak to measure the excitation spectrum reliably. However, there is no other luminescence in the crystal which could contribute to the ODMR effects measured.

The ODMR was also investigated in a crystal which was enriched with the magnetic isotope ^{17}O (Eachus *et al* 1991a,b). However, no hyperfine splitting nor any broadening of the ODMR lines was seen.

3.3. Time-resolved optically detected magnetic resonance measurements

Time-resolved ODMR measurements were carried out by monitoring the time evolution of the luminescence intensity after switching resonant microwaves on and off. Figure 6 shows this for setting the magnetic field into the high-field line at 930 mT for B parallel to the c axis. After switching on the microwaves, a steep rise in the luminescence intensity is

observed which decays after about 3 ms while, after switching off the microwaves, there is a decrease in the luminescence intensity, again levelling out after about 3 ms. The time behaviour after switching off the microwaves has two characteristic times: one of the order of a fraction of a millisecond, and the other of about a millisecond, resembling the two lifetimes measured in luminescence (figure 3). The time evolution of the ODMR signals is analysed in section 4.

At 840 mT, exactly the same time behaviour of the ODMR line was observed.

4. Discussion

4.1. Time-resolved optically detected magnetic resonance measurements

The observed time evolution of the ODMR effect is characteristic for a triplet system in which one of the triplet levels has a fast radiative recombination probability k_i^r compared with the other two. For example, a time behaviour such as that in figure 6 was observed in biacetyl-d_6 molecules (Chan 1982). After switching on the microwaves, the steep rise in luminescence reflects the transfer of spin population from a level with a lower radiative recombination probability to the fast radiative recombination probability, while after switching off the microwaves the decrease in the luminescence intensity is caused by the momentary depletion of spin population as a consequence of the previously enhanced radiative decay during the microwave transition. The solution of the corresponding rate equations (Chan 1982), under the assumption that the spin–lattice relaxation time T_1 is long compared with the lifetimes of the triplet states, gives the following expression for the time evolution of the ODMR effect after the microwave of a saturating transition between levels i and j has been switched off at the time t_0:

$$\Delta I(t) \propto \left(\frac{k_i^r}{k_i} \exp\left(k_i(t-t_0)\right) - \frac{k_j^r}{k_j} \exp\left(k_j(t-t_0)\right) \right). \tag{2}$$

$\Delta I(t)$ is the change in luminescence intensity due to the ODMR effect. k_i and k_j are the total decay probabilities to the ground state of the levels i and j which were connected with a saturating microwave transition before the microwaves were switched off. k_i^r and k_j^r are the radiative parts of the total decay rates. The inverse of the total decay probabilities are the lifetimes τ_1 and τ_2 observed in luminescence.

After switching off the microwaves, the time evolution of the ODMR signal is determined by the decay probabilities k_i and k_j of the two levels which had been connected by the EPR transition. In figure 6 it is shown that the evolution could be simulated by taking the two lifetimes τ_1 and τ_2 determined in the luminescence experiment (figure 3) and by setting the ratio $(k_i^r/k_i)/(k_j^r/k_j)$ of the two amplitudes equal to 1.13, where i is the fast (0.2 ms) and j the slower component (1 ms). This shows that the luminescence and the ODMR are correlated, i.e that the luminescence band is not composed of two different luminescence bands: one with 0.2 ms and one with 1 ms radiative lifetimes. It also follows that for both levels the ratios k_i^r/k_i are about the same. Since the same time evolution was also observed for the lower-field line, the constancy of k_i^r/k_i applies to all three levels. One may speculate that the radiative decay probability is equal to the total decay probability, since the constant ratio applies to both the slow and the fast levels.

As both triplet ODMR transitions ($B = 840$ mT and $B = 930$ mT) show exactly the same time behaviour after switching off the microwaves, two levels must relax with the same time constant. Therefore, two possibilities exist: either there are two fast levels

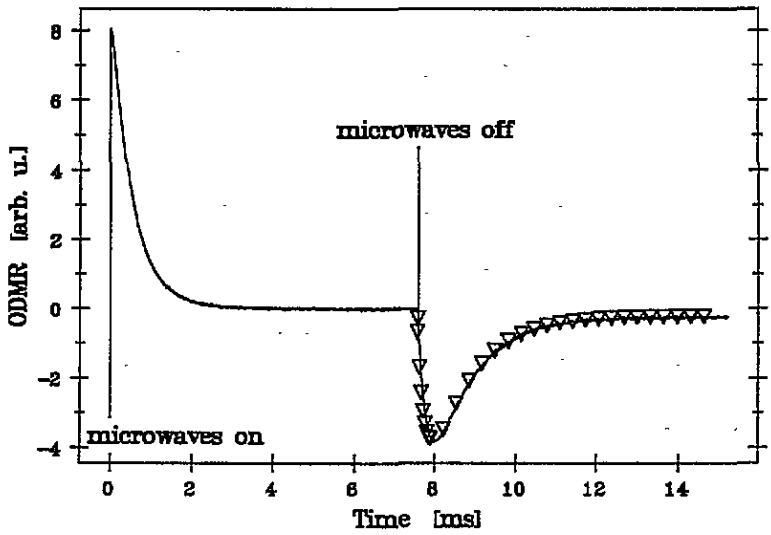

Figure 6. Time-resolved ODMR measurement ($B \parallel c$; $|B| = 930$ mT; $T = 2$ K; $\nu = 23.9$ GHz). The vertical axis shows the relative ODMR effect. The microwaves were switched on at $t = 0$ s. The vertical bar indicates the time of switching off the microwaves after about 8 ms. The transient peak of the ODMR effect is a factor of about 30 larger than the stationary value. The triangles are the calculated transient ODMR effect using the two lifetimes $\tau_1 = 0.2$ ms and $\tau_2 = 1.0$ ms obtained from the luminescence measurements after switching off the microwaves (see text).

($\tau_1 = 0.2$ ms) and one slow level ($\tau_2 = 1$ ms) or vice versa. We assume that the $|\pm 1\rangle$ levels behave similarly so that they decay with the same time constant. We furthermore assume that the pumping rates $P_{\pm 1}$ of the $|\pm 1\rangle$ states are the same and that the total decay probability for the three triplet states is equal to the radiative relaxation probability ($k_i = k_i^r$). Under steady-state irradiation, the population of the triplet levels N_i^0 is related to the population probabilities P_i and decay probabilities k_i in a simple manner: $N_i^0 = P_i/k_i$, $i = +1, 0, -1$. This leads to a steady-state luminescence level $I \propto 2k_{+1}N_{+1}^0 + k_0N_0^0$ ($P_{+1} = P_{-1}$ and $k_{+1} = k_{-1}$). After switching off the excitation light, the luminescence intensity decays as described by

$$I(t) \propto \left(2P_{+1}\ \exp\left(-k_{+1}(t-t_0)\right) + P_0\ \exp\left(-k_0(t-t_0)\right)\right). \tag{3}$$

With these assumptions, the relative amplitude of the two exponentials measured in the luminescence lifetime experiment (figure 3) is equal to $2P_{+1}/P_0$. The measured relation was $A_2(\tau_2 = 1\ \text{ms}/A_1(\tau_1 = 0.2\ \text{ms}) = 1.7$. If we assume that the populating probabilities P_i of all three levels are equal, then we end up with a factor of 2 which is relatively close to 1.7. That would mean that the fast level is the $|0\rangle$ state and the bottlenecks are the $|\pm 1\rangle$ states. We get a value of exactly 1.7 with the condition $P_0 = 1.18P_{+1}$. If we assume that the bottleneck is the $|0\rangle$ state, then the pumping probability P_0 has to be $P_0 = 3.4P_{+1}$.

The excited state has a $^3T_{1u}$ symmetry because of the p hole in the oxygen. Therefore, the bottleneck must be the $m_s = 0$ state, as was found, for example, for the STEs in alkali halides (Song and Williams 1993) or for F centres in CaO (Edel *et al* 1972) which are analogous cases. Consequently, one must conclude that the $|m_s = 0\rangle$ state has a higher population probability than the other two states, by a factor of approximately 3.

4.2. Luminescence

As was seen from table 1, the luminescence at 2.43 eV is not measured when the BaFBr crystal is grown after purification with HF and the luminescence is strong when doping with oxygen. Purification with $SiBr_4$ apparently removes oxygen only from the $BaBr_2$ powder but not from the BaF_2 powder. The oxygen luminescence is weaker in crystals grown with no purification treatment at all, but the oxygen content is estimated to be still in the 100 ppm range (Eachus *et al* 1991a,b). The ODMR comes from an excited triplet state. In principle, a triplet ODMR spectrum could originate from a STE as was speculated by Crawford and Brixner (1989). However, the associated luminescence should not be dependent on oxygen doping or purification. Therefore, we assign the 2.43 eV luminescence band to O^{2-} defects. In addition to triplet luminescence, one expects to see a singlet luminescence band with a shorter radiative lifetime. Within experimental error, such an emission has not been observed.

The possibility of measuring O^{2-} luminescence is important for the improvement in x-ray storage phosphors using BaFBr, since the oxygen content influences the phosphor performance significantly (Spaeth *et al* 1995). The oxygen content must be controlled even at very low level considering the rather low dose of the x-irradiation dose in the medical use of such a phosphor. The O^{2-} luminescence can be measured with a high sensitivity and there is no need for single crystals to do that. We have not been able, however, to calibrate it quantitatively and to determine a lower detection limit.

4.3. O^{2-} centres

From the ODMR we know that there are four centre orientations. The presence of charge-compensating vacancies will determine the orientation of the fine-structure tensor, as will be discussed later. From the present ODMR experiments alone, one cannot decide whether O^{2-} resides on an F^- or Br^- site. For the site assignment we have to use additional information from photochemical reactions involving the O^{2-} centres. When irradiating with UV light into the O^{2-} absorption band at room temperature or by x-irradiation, the crystal turns blue because $F(Br^-)$ centres are formed. O_F^- centres are generated as was shown by EPR, ENDOR and magneto-optical experiments. When generating $F(Br^-)$ centres below 120 K, the $F(Br^-)$ absorption band is slightly shifted to a lower energy, indicating a slightly perturbed Br^- lattice site for the trapped electron. After warming the crystal to room temperature, the absorption band shifts to the higher-energy position which is also found when x-irradiating the crystal at room temperature or additively colouring it. The MDCA-detected EPR line of the $F(Br^-)$ centres does not show any broadening when measured in the slightly shifted MDCA band at low temperature (Eachus *et al* 1991a,b). From these experiments and the O_F^- ENDOR investigation (Eachus *et al* 1991b) it is concluded that O^{2-} is incorporated on the F^- site (see figure 1) and that F centres are produced by trapping electrons in a Br^- vacancy present for charge compensation of the extra charge of O_F^{2-}. It could not be said, however, whether the Br^- vacancy was a nearest or second-nearest neighbour or whether both positions were present as charge-compensating vacancies. The shift of the $F(Br^-)$ band to its normal position after warming the crystal above 200 K was interpreted by the thermally activated diffusion of $F(Br^-)$ centres away from the oxygen into a random Br^- lattice position.

O^{2-} can also be incorporated in Br^- sites as shown by ^{17}O NMR for highly doped crystals (Bastow *et al* 1994) and by EPR and ENDOR of O_{Br}^- centres generated by ionizing radiation (Eachus *et al* 1995). However, O_{Br}^- is not incorporated by back-doping BaO into a purified crystal. Its incorporation seems to proceed via OH^- radicals. In 'normally grown'

BaFBr crystals, O^-_{Br} centres are not found (Eachus *et al* 1995). Thus, we assign the O^{2-} luminescence to O^{2-}_F defects charge compensated by a nearby Br^- vacancy.

4.4. O^{2-}–V^-_{Br} model and electronic structure of the O^{2-} triplet state

We have seen four centre orientations for the triplet state O^{2-}. Each centre orientation can be transformed into the other three by applying the mirror symmetry of the c–a and/or c–b planes. Thus, the O^{2-} triplet state is associated either with a nearest (Br_I) or a second-nearest (Br_{II})Br^- vacancy. The O^{2-}_F ion is correlated to one of the two Br^- vacancies. We shal discuss below which of the two possibilities is the more likely.

The zero-field parameter D contains two parts: $D = D_{ss} + D_{so}$, whereby D_{ss} is due to the spin–spin interaction and D_{so} due to the spin–orbit interaction (see, e.g., Song and Williams (1993)). D_{so} depends on the spin–orbit interaction which is probably small for the p hole in O^-, for which data do not exist. Spin–orbit data for similar atoms, such as F^0 (404 cm^{-1}), Ne^+ (782 cm^{-1}), Na^{2+} (1364 cm^{-1}) (*Atomic Energy Levels* vol 1 1971) suggest it to be around 400 cm^{-1}. Thus, similarly as in the STEs in alkali fluorides, D_{so} can be neglected compared with D_{ss} (Song *et al* 1990).

The optically excited electron will be in an s-like state; the hole is an O^- 2p hole. An electronic configuration, in which an excited s-like electron is centred at the O^-_F site, must be excluded, because the dipole–dipole interaction (spin–spin interaction) would then yield an axially symmetric zero-field splitting tensor, which is not observed; the asymmetry of D is quite substantial ($E \approx \frac{1}{4}D$). Likewise, an off-centre geometry between the s electron and the p hole, in which both are aligned along the same axis, would yield an axially symmetric D tensor. Therefore, the electronic configuration must be such that the excited electron is displaced from the O^- 2p hole lobe axis in a way that the connection line between O^- and the electron location makes a non-zero angle with respect to the fine structure tensor axis.

The nearest and second-nearest Br^- vacancies have an attractive potential for the excited electron and a repulsive potential for the positive O^- 2p hole. Thus, a configuration in which the excited state of the system consists of an F(Br^-) centre in the nearest or second-nearest position and a p hole with its lobe essentially perpendicular to the connection line between O^-_F and the vacancies would be a possibility. In figure 7 these two configurations are sketched. The connection line to the Br_{II} vacancy makes, indeed, an angle of 90° with the z axis of the D tensor (henceforth called the 'perpendicular configuration'), while that of the Br^-_I vacancy makes an angle of about 75° (henceforth called the 'oblique configuration'). For both configurations, the dipole–dipole interaction would lead to a non-axially symmetric zero-field splitting tensor as was observed. We have estimated the axial part of D_{ss} (D_{zz}) for these two configurations assuming Gaussians ($\exp^{(-\alpha r^2)}$) for the wavefunctions for both the p hole and the F(Br^-) centres by calculating the dipole–dipole interaction between them. For the hole we assumed that $\alpha_h = 0.3$ au, while α_e of the F centre was varied. This α_h was often used to describe STEs. The regular lattice site of the Br_I vacancy is 7 au away from O^-_F; that of the Br_{II} 10 au (table 3; see also figure 7).

For $\alpha_e \approx 0.08 \pm 0.01$, optimized in previous work on F centres in SrF_2 (Adair *et al* 1985) and SrFBr (Baetzold and Song 1993), we obtain the right order of magnitude for D_{ss} which shows that the assumption of an F(Br^-) centre–O^-_F pair seems reasonable (table 3). To decide between the two possibilities, we have to invoke further properties of the system.

In order to help to decide between the two geometries, we have estimated the D_{ss}-values for various separations and orientations about the ideal values, as indicated in figure 7. The method used for this evaluation has been given by Song *et al* (1990) and Leung *et al* (1992). An attempt to estimate the lifetimes of the triplet state by analogy with the case of the off-centre STE in alkali halides (Song and Williams 1993) gave results which are not

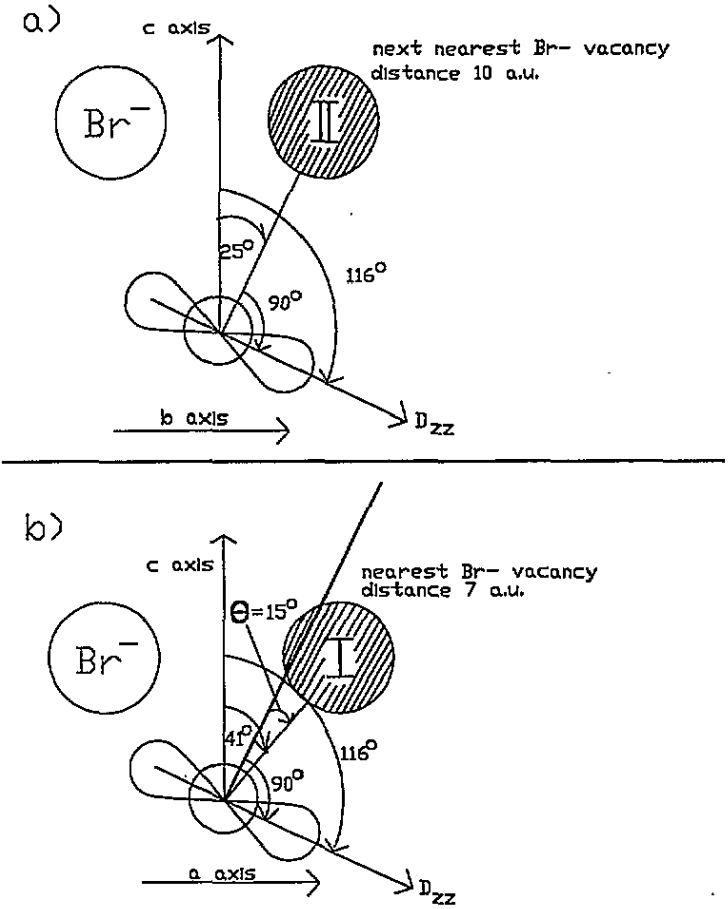

Figure 7. (a) Position of the z axis of the fine-structure tensor relative to the position of the second-nearest Br^- vacancy (shaded) in the c–b mirror plane. The other second-nearest Br^- ion in that plane is also indicated. (b) Position of the z axis of the fine structure tensor relative to the position of the nearest Br^- vacancy (shaded) in the c–a mirro plane. The other nearest Br^- ion in that plane is also indicated.

Table 3. Theoretical estimates of the fine-structure parameter D_{ss}. The angle θ is indicated in figure 7(b).

Perpendicular cases		Oblique cases		
d (au)	D_{ss} (mT)	d (au)	θ (deg)	D_{ss} (mT)
9	146	6.5	15	280.7
10	109	6.5	34	77
11	83	7.5	15	203.5
11.3	77	7.5	31	77
12	64.7	8.5	15	145
		8.5	28	77
		9.5	15	105.3
		9.5	23	77

conclusive enough to choose between the two geometries. However, it is interesting to note that the lifetimes obtained in the present work are of comparable magnitude as that of the triplet STE states in NaF: 1.58×10^{-3} s and 3.43×10^{-4} s (Tanimura 1995).

From this table it appears that the second-nearest neighbour site seems more reasonable. The D-value is more in agreement with the observed value at a distance of about 11 au. For the first-neighbour site, at a distance of about 7 au and an angle of about 15° off the normal to the p lobe, the D-value evaluated is off by as factor of as much as 3. To fit the D-value, the angle has to be increased to about 30°. The lifetime τ is not very sensitive within a relatively small range of distance and, therefore, is not a critical factor.

5. Conclusion

In conclusion we have found that the excited triplet state of O_F^- in BaFBr is a pair consisting of an O_F^- and an $F(Br^-)$ centre. Our estimates favour the second-nearest Br^- vacancy to be the location of the F centre.

References

Abragam A and Bleaney B 1986 *Electron Paramagnetic Resonance of Transition Ions* (New York: Dover)

Adair M, Leung C H and Song K S 1985 *J. Phys.: Condens. Matter* **18** 2909

Ahlers F J, Lohse F, Spaeth J-M and Mollenauer L F 1983 *Phys. Rev.* B **28** 1249

Atomic Energy Levels vol 1971 (Washington, DC: National Bureau of Standards)

Baetzold R C and Song K S 1993 *Phys. Rev.* B **48** 14907

Bastow T J, Stuart S N, McDugle W G, Eachus R S and Spaeth J-M 1994 *J. Phys.: Condens. Matter* **6** 8633

Beck H P 1979 *Z. Anorgan. (Allg.) Chem.* **451** 73

Chan I Y 1982 *Triplet State ODMR Spectroscopy* ed R H Clark (New York: Wiley) ch 1

Crawford M K and Brixner L H 1989 *J. Appl. Phys.* **66** 15

Eachus R S, McDugle W G, Nuttal R H D, Olm T, Koschnick F K, Hangleiter Th and Spaeth J-M 1991a *J. Phys.: Condens. Matter* **3** 9327–38

—— 1991b *J. Phys.: Condens. Matter* **3** 9339–49; 1995 *Phys. Rev.* B submitted

Edel P, Hennies C, Merle d'Aubigné Y, Romestin R and Tawarowski Y 1972 *Phys. Rev. Lett.* **28** 1268

Koschnick F K 1991 *PhD Thesis* Paderborn

Koschnick F K, Hangleiter Th, Spaeth J-M and Eachus R S 1992 *J. Phys.: Condens. Matter* **4** 3001

Leung C H, Zhang C G and Song K S 1992 *J. Phys.: Condens. Matter* **4** 1489

Liebig B W and Nicollin D 1977 *Acta Crystallogr.* B **33** 2790

Song K S, Leung C H and Spaeth J-M 1990 *J. Phys.: Condens. Matter* **2** 6373

Song K S and Williams R T 1993 *Self-trapped Excitons (Springer Series of Solid State Sciences 105)* (Berlin: Springer) ch 5

Spaeth J-M, Hangleiter Th, Koschnick F K and Pawlik Th 1995 *Radiat. Eff. Defects Solids* **133–4**

Tanimura K 1995 unpublished